View metadata, citation and similar papers at core.ac.uk

brought to you by CORE

provided by ScholarWorks@UNIST

AIP Journal of Applied Physics

Soft x-ray resonant magneto-optical Kerr effect as a depth-sensitive probe of magnetic heterogeneity: A simulation approach

Ki-Suk Lee, Dae-Eun Jeong, Sang-Koog Kim, and J. B. Kortright

Citation: Journal of Applied Physics **97**, 083519 (2005); doi: 10.1063/1.1861969

View online: http://dx.doi.org/10.1063/1.1861969

View Table of Contents: http://scitation.aip.org/content/aip/journal/jap/97/8?ver=pdfcov

Published by the AIP Publishing

Articles you may be interested in

Bragg magneto-optical Kerr effect measurements at Co stripe arrays on Fe(001)
J. Appl. Phys. **97**, 073909 (2005); 10.1063/1.1868853

Soft x-ray resonant magneto-optical Kerr effect as a depth-sensitive probe of magnetic heterogeneity: Its application to resolve helical spin structures using linear p polarization
J. Appl. Phys. **96**, 7414 (2004); 10.1063/1.1806535

Atomic-scale depth selectivity of soft x-ray resonant Kerr effect
Appl. Phys. Lett. **83**, 3764 (2003); 10.1063/1.1622123

Soft x-ray longitudinal magneto-optical Kerr effect measured from Co/Cu multilayers at the Co L 2,3 edges
J. Appl. Phys. **93**, 6516 (2003); 10.1063/1.1555320

Kerr imaging of a Co/Pt bimodal magneto-optical medium
J. Appl. Phys. **85**, 5169 (1999); 10.1063/1.369113

[This article is copyrighted as indicated in the article. Reuse of AIP content is subject to the terms at: http://scitation.aip.org/termsconditions. Downloaded to] IP: 114.70.7.203 On: Mon, 27 Oct 2014 02:28:35

HTML ABSTRACT + LINKS

Soft x-ray resonant magneto-optical Kerr effect as a depth-sensitive probe of magnetic heterogeneity: A simulation approach

Ki-Suk Lee, Dae-Eun Jeong, and Sang-Koog Kim[a)]
Nanospintronics Laboratory, School of Materials Science and Engineering, and Research Institute of Advanced Materials, Seoul National University, Seoul 151-744, Korea

J. B. Kortright
Materials Sciences Division, Lawrence Berkeley National Laboratory, University of California, One Cyclotron Road, Berkeley, California 94720

(Received 3 September 2004; accepted 24 December 2004; published online 6 April 2005)

We report a noticeable depth sensitivity of soft x-ray resonant magneto-optical Kerr effect able to resolve depth-varying magnetic heterostructures in ultrathin multilayer films. For various models of depth-varying magnetization orientations in an ultrathin Co layer of realistic complex layered structures, we have calculated the Kerr rotation, ellipticity, intensity spectra versus grazing incidence angle ϕ, and their hysteresis loops at different values of ϕ for various photon energies $h\nu$'s near the Co resonance regions. It is found from the simulation results that the Kerr effect has a much improved depth sensitivity and that its sensitivity varies remarkably with ϕ and $h\nu$ in the vicinity of the resonance regions. These properties originate from a rich variety of wave interference effects superimposed with noticeable features of the refractive and absorptive optical effects near the resonance regions. Consequently, these allow us to resolve depth-varying magnetizations and their reversals varying with depth in a single magnetic layer and allow us to distinguish interface magnetism from the bulk properties in multilayer films. In this paper, the depth sensitivity of the Kerr effect with an atomic-scale resolution is demonstrated and discussed in details in several manners with the help of model simulations for various depth-varying spin configurations. © *2005 American Institute of Physics*. [DOI: 10.1063/1.1861969]

I. INTRODUCTION

At the core of current issues in the research area of magnetism and magnetic materials are ultrathin films of magnetic multilayer structures as well as their intriguing magnetic properties associated closely with their characteristic structures.[1] The reason is such films and their properties are currently (or in the near future) applicable to sophisticated ultrahigh-density information storage[2] and other spintronic devices.[3] Such multilayer films consist of two or more ultrathin layers of different types of nonmagnet, insulator, ferromagnet (F), antiferromagnet (AF), superconductors, etc.[1] Many interesting phenomena in such hybrid structures are relevant to a rich variety of magnetic interactions with their multiple length scales, as well as intrinsically modified electronic structures at interfaces.[1,4,5]

Fundamental magnetic properties, such as the magnitude and orientation of magnetizations in heteromagnetic structures, can differ in depth and/or from the interface to the interior of each constituent layer.[1,6] The overall properties can thus be characterized by magnetic microstructures at interfaces inherent in the layered structure and/or depth-varying properties in each constituent layer. As the thicknesses of the constituent layers approach nanometer scale or even less, the depth-dependent structures and interface magnetism become more crucial in determining the overall properties. Details of chemical and magnetic structures varying in depth on the atomic-scale levels must thus be identified to understand the causes of the overall magnetic properties.

It is a challenge to characterize depth-varying magnetic structures as well as to discriminate an interface contribution from the bulk ones. Recently, soft x-ray resonant Kerr effect relying on intensity measurements of reflected waves becomes one of the newly emerging techniques as a depth-sensitive probe.[7–9] One of the great advantages of this spectroscopic probe is the element specificity able to resolve separately the magnetic properties of each constituent element in multicomponent magnetic films.[7,10] This element selectivity is possible due to a large electric dipole transition from the spin-orbit split initial states of core electrons to the highly unoccupied spin-polarized final states in the resonance edges.[11] In addition, the strong resonance features lead to a rich variety of refractive and absorptive optical behaviors and consequently yield a remarkably variable interference effect in ultrathin films depending on the grazing angle of incidence (ϕ) as well as photon energy ($h\nu$) in the vicinity of the resonance regions.[7,12] These properties can hence provide a much improved depth sensitivity and its dependence on ϕ and $h\nu$ into the x-ray resonant magneto-optical Kerr effect (MOKE).

In this paper, soft x-ray resonant MOKE is discussed in details in the light of its depth sensitivity as a probe of heteromagnetic structures. This technique has a few advantages over other spectroscopic tools, such as soft x-ray photoemission and absorption spectroscopies, which are based on electron yield detection and therefore have a limited $1/e$ probing

[a)]Author to whom correspondence should be addressed; electronic mail: sangkoog@snu.ac.kr

 © 2005 American Institute of Physics

[This article is copyrighted as indicated in the article. Reuse of AIP content is subject to the terms at: http://scitation.aip.org/termsconditions. Downloaded to] IP: 114.70.7.203 On: Mon, 27 Oct 2014 02:28:35

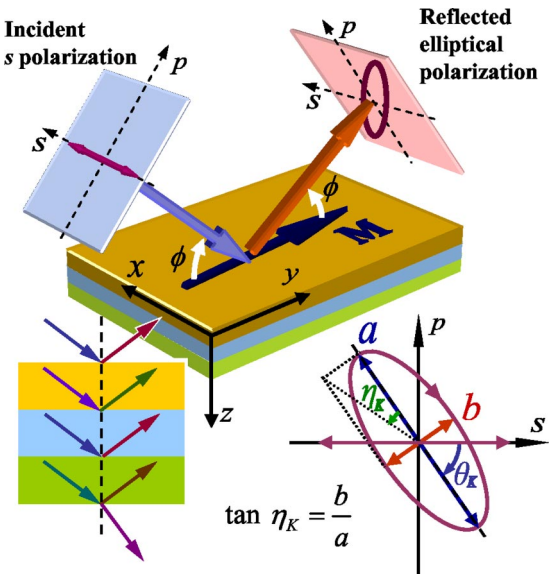

FIG. 1. (Color online) A graphical illustration of the longitudinal Kerr effect, where the magnetization orientation lies in the film plane and the scattering plane (the *y*-*z* plane). For incident *s*-polarized waves, the θ_K and η_K of reflected waves are defined in the inset.

depth (below 50 Å) and some artifacts in the measurement under an applied magnetic field.[13] In contrast, soft x-ray resonant Kerr effect allows us to resolve depth-varying magnetic structures and properties in *buried* layers and magnetic structures *localized at interfaces* even under *a strong magnetic field* in a relatively straightforward and simple manner. Recently, we reported a much improved depth sensitivity of the Kerr effect in the Co resonance region demonstrated with a real sample exhibiting depth-varying magnetization reversals in a 35-Å-thick Co layer.[12] Here, we report our work extended into elaborate studies of the depth-resolving capability of the resonant Kerr effect through various model calculations. Based on simulation results, a large depth sensitivity of the Kerr effect, its variation with ϕ and $h\nu$, and the atomic-scale depth selectivity are verified. Moreover, as a guide for the studies of magnetic properties via soft x-ray MOKE, we present many useful MOKE techniques demonstrated from some specific model calculations, which can be applied to investigate real, inhomogeneous magnetic films.

This paper is organized as follows. Section II reviews theoretical descriptions of MOKE. Section III presents calculation results and resonant magneto-optical properties in the light of a depth selectivity of the Kerr effect. In Sec. IV, possible depth-varying spin structures in realistic samples are discussed. Finally, Sec. V summarizes this work.

II. THEORETICAL DESCRIPTIONS OF MOKE

MOKE intrinsically originates from the incorporation of both the differential absorption and refraction of opposite circular components of waves. These give rise to various changes in the polarization state as well as the intensity of reflected waves depending on the magnitude and orientation of a certain magnetic moment, as depicted in Fig. 1. The polarization state is characterized by measurable Kerr rotation θ_K and ellipticity η_K as defined in Fig. 1. To estimate those classical and macroscopic values for an incident wave with a linear polarization in response to a magnetic film, standard formalisms typically used in visible wavelengths are extended into soft x-ray energy regions. The dielectric tensor that represents optical and magneto-optical characteristics of a certain magnetic film is thus used to calculate soft x-ray MOKE.

For an arbitrary magnetization **M**, the dielectric tensor is given as[14]

$$\varepsilon(h\nu) = n_0^2 \begin{bmatrix} 1 & -iQm_z & iQm_y \\ iQm_z & 1 & -iQm_x \\ -iQm_y & iQm_x & 1 \end{bmatrix},$$

where $m_{x,y,z}$ are the **M** components projected along the x,y,z axes defined as in Fig. 1 and the *y*-*z* plane is the scattering plane. Q is the Voigt constant and n_0 is the pure charge forward scattering, and both are a function of $h\nu$. Here, a first-order approximation is considered for Q. The dielectric tensor is related to the complex refractive index, $n(h\nu)=1-\delta(h\nu)+i\beta(h\nu)=\sqrt{\varepsilon(h\nu)}$. For left- and right-handed circular components, their refractive indices are given as $n_\pm(h\nu)=1-\delta_\pm(h\nu)+i\beta_\pm(h\nu)$, and hence $Q=2(n_+-n_-)/(n_++n_-)$. For calculations of the θ_K, η_K, and Kerr intensity I_K of a wave reflected from a magnetic sample, the Kerr matrix R_{sp} based on the linear (s,p) polarization mode of both incident and reflected waves has been widely used as follows:[15,16]

$$\begin{pmatrix} E_s^r \\ E_p^r \end{pmatrix} = R_{sp} \begin{pmatrix} E_s^i \\ E_p^i, \end{pmatrix},$$

where

$$R_{sp} = \begin{pmatrix} r_{ss} & r_{sp} \\ r_{ps} & r_{pp} \end{pmatrix}.$$

The reflected and incident electric fields $E_{s(p)}^r$ and $E_{s(p)}^i$ of an $s(p)$ component are related to each other through R_{sp}, where $r_{ab} \equiv E_a^r/E_b^i$ is the reflection coefficient for incident (i) "b" and reflected (r) "a" polarizations (a, $b=s$ or p). The off-diagonal terms lead to the complex Kerr rotation angle by a relation of $\Phi_K=\theta_K+i\eta_K \simeq -r_{ps}/r_{ss}$, and $I_K=|E_s^r|^2+|E_p^r|^2$. For a given polarized wave of incidence, the varying polarization state of a reflected wave can thus be obtained from (or determine) θ_K, η_K, and I_K values.

To calculate the Co resonant Kerr effect from multilayer structures, such as NiFe/FeMn/Co/Pd, the numerical values of Co $n_\pm$ are necessary in a broad range of $h\nu$ covering the Co L_3 and L_2 edges. In Fig. 2 are shown the experimental data of Co $n_\pm$, which were obtained from $\beta_\pm$ measured through magnetic circular dichroism (MCD) and $\delta_\pm$ determined from the Kramers–Kronig transformation (KKT) of the values of $\beta_\pm$.[17] As for the values of n of other elements, such as Fe, Ni, and Pd around the Co absorption edges, tabulated Henke data were used because these values can be well predicted in the nonresonance regions of these individual elements.[18]

[This article is copyrighted as indicated in the article. Reuse of AIP content is subject to the terms at: http://scitation.aip.org/termsconditions. Downloaded to] IP: 114.70.7.203 On: Mon, 27 Oct 2014 02:28:35

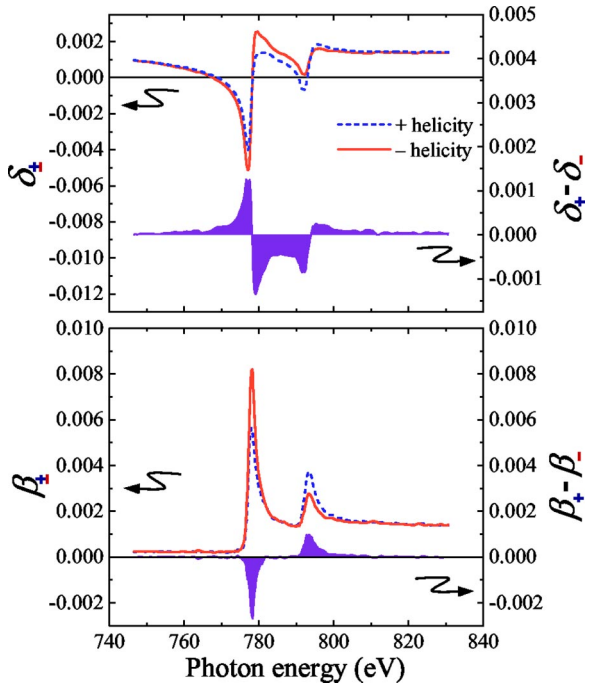

FIG. 2. (Color online) Photon helicity-dependent complex refractive index of Co ($n_{\pm}=1-\delta_{\pm}+i\beta_{\pm}$). Experimentally measured values of $\beta_{\pm}$ are Kramer–Kronig transformed to yield the corresponding values of $\delta_{\pm}$.

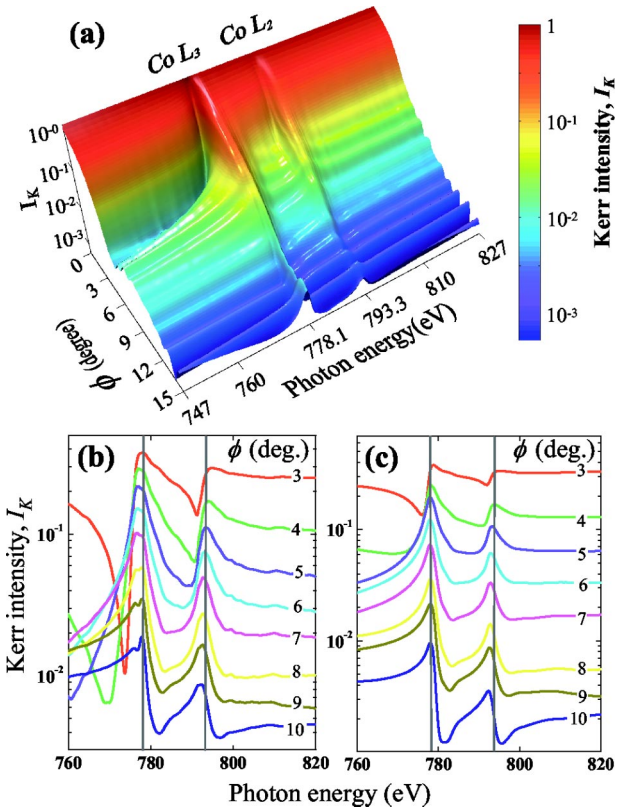

FIG. 3. (Color online) Calculations of reflected intensity spectra in the $h\nu$ range of the Co L_3 and L_2 edges as a function of ϕ using *s*-polarized incident x rays. The model structure used is the same as that of a real sample, Si / SiO_2(1500 Å)/Ta(50 Å)/$Ni_{81}Fe_{19}$(80 Å)/$Fe_{50}Mn_{50}$(200 Å)/Co(35 Å)/Pd(15 Å) (Ref. 12). (a) presents a surface plot of those values against both ϕ and $h\nu$. (b) shows the reflectivity spectra as a function of $h\nu$ for different values of ϕ as noted. The calculated intensities in (b) are compared with those shown in (c) measured from the real sample (see Ref. 12). The intensity data are plotted on a logarithmic scale to compare all the spectra for the different values of ϕ.

III. SIMULATION RESULTS

A. Calculations of I_K, θ_K, and η_K spectra

I_K spectra versus both ϕ and $h\nu$ in a range of covering the Co L_3 (778.1 eV) and L_2 (793.3 eV) edges are calculated for the *s* linear polarization, as shown in Figs. 3(a) and 3(b). The resultant I_K spectra exhibit strong resonance features around the Co L_3 and L_2 edges. These resonance features are similar to the dispersive feature of δ for lower ϕ but become somewhat similar to the absorptive feature of β for higher ϕ. The resonance behavior becomes more complicated in an intermediate range of ϕ due to the large contributions of refractive and absorptive behaviors in the vicinity of the absorption edges (see Fig. 2). It is known that the refractive and absorptive parts of the complex refractive index lead to remarkable variations of the penetration depth as well as interference effect of propagating waves around the resonance regions.[7] For given $h\nu$'s, the I_K spectra versus ϕ show oscillatory behaviors, which are associated with the interference effect in the layered structure of this model system. The interference effect superimposed with the strong resonance features, which varies with ϕ and $h\nu$, could give rise to a depth sensitivity of x-ray resonant MOKE.

Some of calculated I_K spectra for several ϕ's are compared to those spectra [Fig. 3(c)] measured from a real sample with the same structure as the model structure. They are both in general agreements. The common features between the two are the resonant features of the reflected intensities around the Co L_3 and L_2 edges, resembling the dispersive feature of absorptive and refractive optical behaviors. In contrast, deep valleys below the Co L_3 edge for $\phi=3°$, 4°, and 5° in the calculated I_K are somewhat different from the corresponding experimental spectra. This is likely to be ascribed to a partial oxidation incorporated at the Co/FeMn interface of the real sample during its preparation. The good agreements between the calculated and measured intensities confirm that this calculation of the Kerr effect from model magnetic heterostructures is promisingly reliable to study/clarify a depth sensitivity of the resonant MOKE and its variations with ϕ and $h\nu$.

Figure 4 shows the calculated values of θ_K and η_K spectra displayed by a surface plot versus both ϕ and $h\nu$. As mentioned above, strong resonance features are obviously seen around the Co L_3 and L_2 edges and are dependent on ϕ as well. For clarity, we also replot some spectra versus $h\nu$ for several different values of ϕ, as shown in the middle and bottom panels of Fig. 4. In those spectra of θ_K, some appear to resemble a general shape of MCD spectra (i.e., $\beta_+-\beta_-$), while some in the η_K spectra do that of Faraday rotation spectra (i.e., $\delta_+-\delta_-$). While KKT directly relates the Faraday rotation with the MCD spectra for the case of transmitted intensity, as revealed in Fig. 3 of Ref. 7, the θ_K and η_K spectra in the case of reflection are not correlated entirely by the KKT. However, it is interesting that the absorptive and refractive features in those spectra are likely to be related partially through the KKT.

[This article is copyrighted as indicated in the article. Reuse of AIP content is subject to the terms at: http://scitation.aip.org/termsconditions. Downloaded to] IP: 114.70.7.203 On: Mon, 27 Oct 2014 02:28:35

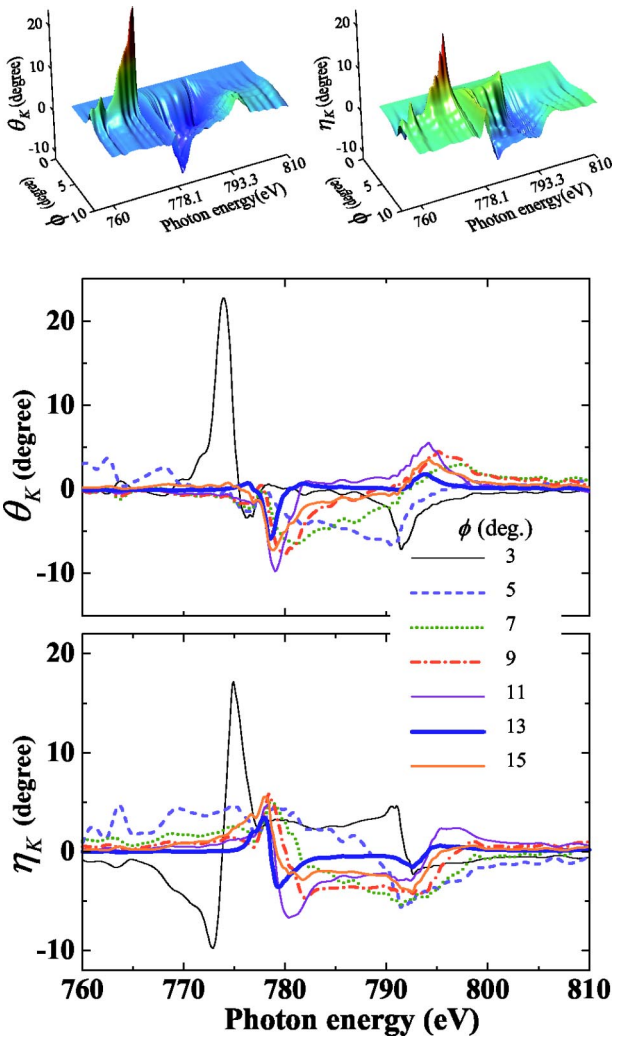

FIG. 4. (Color online) Calculated spectra of θ_K and η_K as a function of ϕ and $h\nu$ in the vicinity of the Co L_3 and L_2 edges from the same model structure as that noted in Fig. 3. In these calculations, the Co magnetization is assumed to be oriented uniformly through the entire thickness of Co. In the bottom panel, the θ_K and η_K spectra are redrawn as a function of $h\nu$ for several values of ϕ as noted.

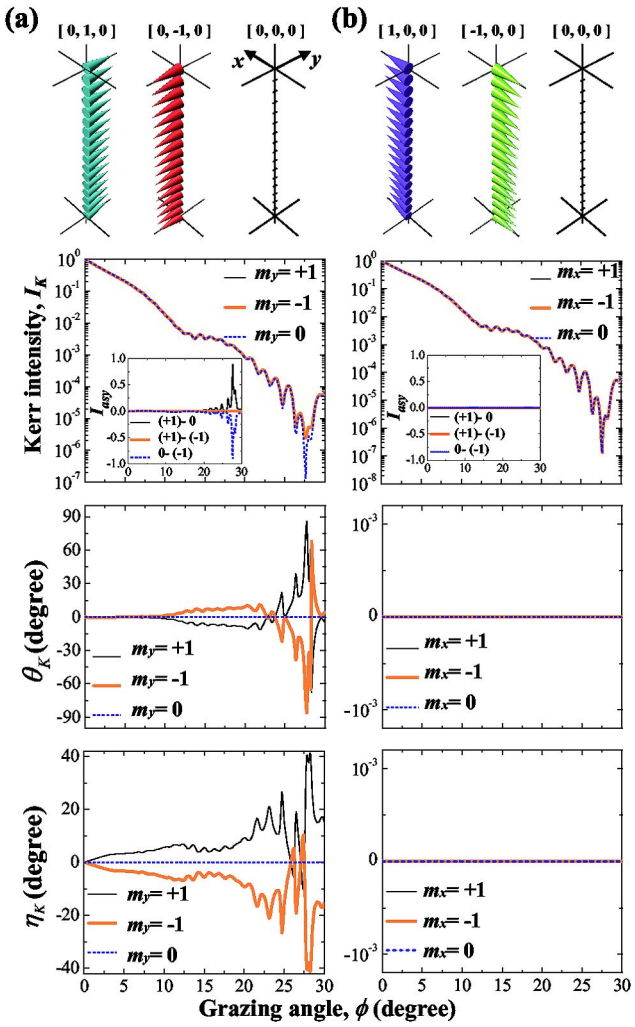

FIG. 5. (Color online) Top panels of (a) and (b) illustrate model spin configurations uniformly oriented through the entire Co thickness. The **M** orientations are denoted as $[m_x, m_y, m_z]$ with each component of $m_{x(y,z)}$ along x (y,z) axis. In (a), m_y varies as +1, −1, and 0 with $m_x = m_z = 0$. In (b), m_x varies as +1, −1, and 0 with holding $m_y = m_z = 0$. The second row panels show I_K and I_{asy} spectra as a function of ϕ at the Co L_3 edge. The third and the last row panels show the corresponding results of θ_K, and η_K, respectively.

Here, we like to stress two things about the resonance features in the θ_K and η_K spectra. First, the strong resonant behaviors in those spectra around the Co-specific L_3 and L_2 edges can give rise to enhanced or reduced contrasts in θ_K and η_K signals for oppositely oriented magnetization reversals, which offer a large magnetic sensitivity as well as the element specificity under appropriate conditions of the measurement. This allows us to resolve magnetization reversals of specific elements of interest with its large sensitivity in multicomponent magnetic samples. Second, the magnitude and sign of θ_K and η_K signals vary remarkably with both ϕ and $h\nu$. This implicates that, depending on which values of ϕ and $h\nu$ are chosen in the measurements, the θ_K and η_K signals can be enhanced or diminished or changed even in their sense. Thus, much care should be taken when one measures magnetization loops through the θ_K and η_K signals. This point indicates somewhat a weakness of the x-ray MOKE techniques as a probe of magnetic structure and properties. However, this can be used as one of the great advantages of the x-ray resonant MOKE in order to resolve depth-varying magnetizations in heteromagnetic structures, which will be discussed in more details hereafter.

B. Dependence of I_K, θ_K, and η_K on the in-plane M components

First, to elucidate how soft x-ray resonant Kerr effect for a linear *s* polarization is sensitive to a magnetization state, we present how I_K, θ_K, and η_K spectra versus ϕ at the Co L_3 edge are sensitive to the in-plane components of **M**. In the present study, we focus only on the sensitivity to the sign and magnitude of the longitudinal and transverse components of **M** uniformly oriented through the thickness of a magnetic layer. In Fig. 5(a), three different configurations are illustrated with a notion of $[m_x, m_y, m_z]$. In the left panel, only the longitudinal **M** component m_y varies as +1, −1, and 0 with $m_x = m_z = 0$, while in the right panel only the transverse component m_x varies as +1, −1, and 0 with $m_y = m_z = 0$. The re-

[This article is copyrighted as indicated in the article. Reuse of AIP content is subject to the terms at: http://scitation.aip.org/termsconditions. Downloaded to] IP: 114.70.7.203 On: Mon, 27 Oct 2014 02:28:35

sultant I_K, θ_K, and η_K spectra versus ϕ calculated from each configuration are shown in the second, third, and last panels in Fig. 5, respectively. It is found that I_K spectra are equal for $m_y=-1$ and $+1$, but different for $|m_y|=1$ and $m_y=0$, as confirmed by their asymmetry spectra of $I_{\text{asy}}=(I_a-I_b)/(I_a+I_b)$ shown in the inset. While the resonant I_K signal for *a linear s polarization* has a sensitivity only to the change of the magnitude of m_y, the corresponding θ_K and η_K signals are remarkably sensitive to the change in both the size and sense of m_y. In contrast with the longitudinal case, I_K, θ_K, and η_K signals for the transverse cases have no any sensitivity to changes in the sign and magnitude of m_x. The remarkable sensitivity of θ_K and η_K to the opposite sense and magnitude of m_y at the resonance edge allows us to resolve spin structures with respect to m_y, but the investigation of m_x variations is hindered for the use of *s*-polarized incident waves.

C. Depth sensitivity of soft x-ray resonant MOKE

As mentioned earlier, a wide variety of the interference effects superimposed with the resonant optical effect can yield a much improved depth sensitivity of the MOKE. Here we verify the capability of the Kerr effect as a depth-sensitive probe of magnetic heterogeneity. As demonstrated with real samples of a multilayer structure in earlier work,[12] magnetization reversals varying with depth can be resolved through θ_K and η_K signals by choosing appropriate values of $h\nu$ and ϕ in those measurements. To understand how the Kerr effect is sensitive to the depth in a given ultrathin layer, first we consider the calculated values of θ_K and η_K vs $h\nu$ and ϕ from a spin-flip model illustrated in Fig. 6(a). In this model, the given Co thickness is divided into three different regions with an equal thickness. The in-plane longitudinal orientations of **M** in each imaginary region are assumed to be incoherently flipped from one direction to the other opposite. This model implies that only the m_y exists during **M** reversals. Here, we consider the depth sensitivity of the resonant Kerr effect just for linearly *s*-polarized waves with respect to m_y. Figures 6(b) and 6(c) show contour plots of the resultant values of θ_K and η_K, respectively, against both $h\nu$ and ϕ, calculated from individual spin configurations noted as S_1, S_2, S_3, and S_4 in Fig. 6(a). The contrasts in the θ_K and η_K values between successive spin structures (i.e., $\Delta\theta_K=\theta_K^{S2}-\theta_K^{S1}$, $\theta_K^{S3}-\theta_K^{S2}$, $\theta_K^{S4}-\theta_K^{S3}$) indicate contrasting $\Delta\theta_K$ for individual spin flips from one direction to the other opposite in the three different regions of top, middle, and bottom depths, which are shown in Fig. 6(d). The value of $\theta_K^{S4}-\theta_K^{S1}$ represents the θ_K contrast for simultaneous spin flips in the three different regions, i.e., the entire Co layer. η_K contrasts are also shown in Fig. 6(e), and analogous interpretations can be made as well. From these calculations, it is evident that $\Delta\theta_K$ and $\Delta\eta_K$ values are changing with depth at which spins are flipped, and these are remarkably changing with ϕ and $h\nu$. This indicates that the resonant MOKE has a significant depth sensitivity varying with ϕ and $h\nu$. This sensitivity is noticeably changing in the vicinity of the Co L_3 and L_2 edges.

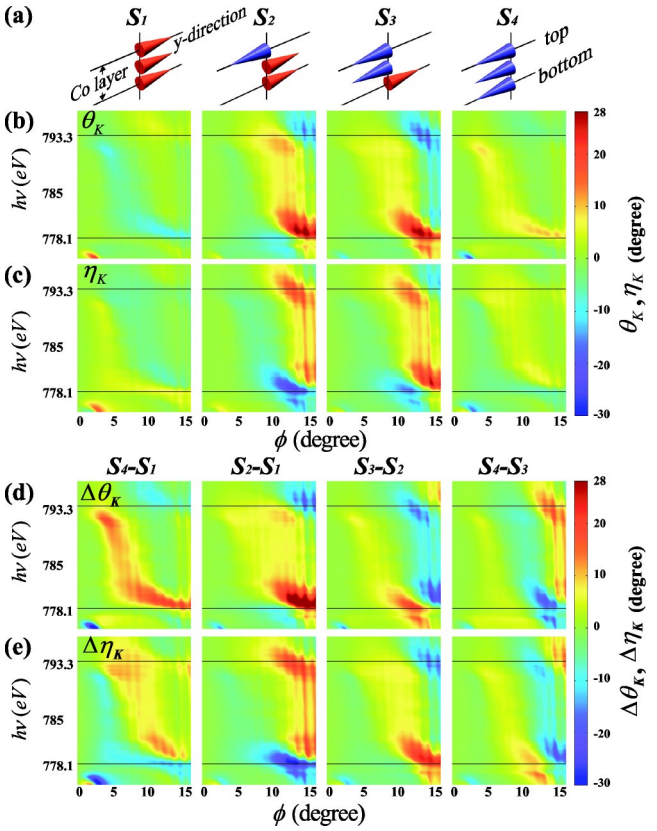

FIG. 6. (Color online) (a) Spin configurations in a single Co layer that is imaginarily divided into three different depth regions. (b) and (c) show contour plots of the calculated values of θ_K and η_K against ϕ and $h\nu$ from those spin structures shown in (a). The contrasts, i.e., $\Delta\theta_K$ and $\Delta\eta_K$ for individual spin flips $(S_2-S_1, S_3-S_2, S_4-S_3)$ in the three different regions are also shown in (d) and (e), respectively. The values of $\Delta\theta_K$ and $\Delta\eta_K$ for S_4-S_1 correspond to those for a simultaneous spin flip through the entire Co layer.

Taking a closer look at the values of $\Delta\theta_K$ around the Co L_3 edge in a range of $\phi=10°\sim15°$, the changes of its magnitude and sign are noticeably different for the top, middle, and bottom layers' spin flips. The zero value for specific depth regions implies that the spin flip at the corresponding depth cannot be detected from the measurement at the given conditions of ϕ and $h\nu$. The changing values of the magnitude and sign on the ϕ-$h\nu$ plane represent a measure of the depth sensitivities of θ_K and η_K signals varying with ϕ and $h\nu$.

Next, to examine the resolution of the found depth sensitivity, we calculate $\Delta\theta_K$ and $\Delta\eta_K$ values for individual spin flips of finely divided 17 layers in a 35-Å-thick Co layer, as shown in Fig. 7. The resultant contrasts for the individual regions are quite different and remarkably vary with ϕ. As ϕ increases, the depth sensitivity increases significantly. These plots clearly reveal that the different weights of the MOKE effect contributed from individual depths offer a much improved depth sensitivity into the resonant MOKE possibly with an atomic-scale resolution.

D. A graphical representation of the Kerr vector on the θ_K-η_K plane

To clarify the depth sensitivity of θ_K and η_K signals found using a spin-flip model, we further consider a graphi-

[This article is copyrighted as indicated in the article. Reuse of AIP content is subject to the terms at: http://scitation.aip.org/termsconditions. Downloaded to] IP: 114.70.7.203 On: Mon, 27 Oct 2014 02:28:35

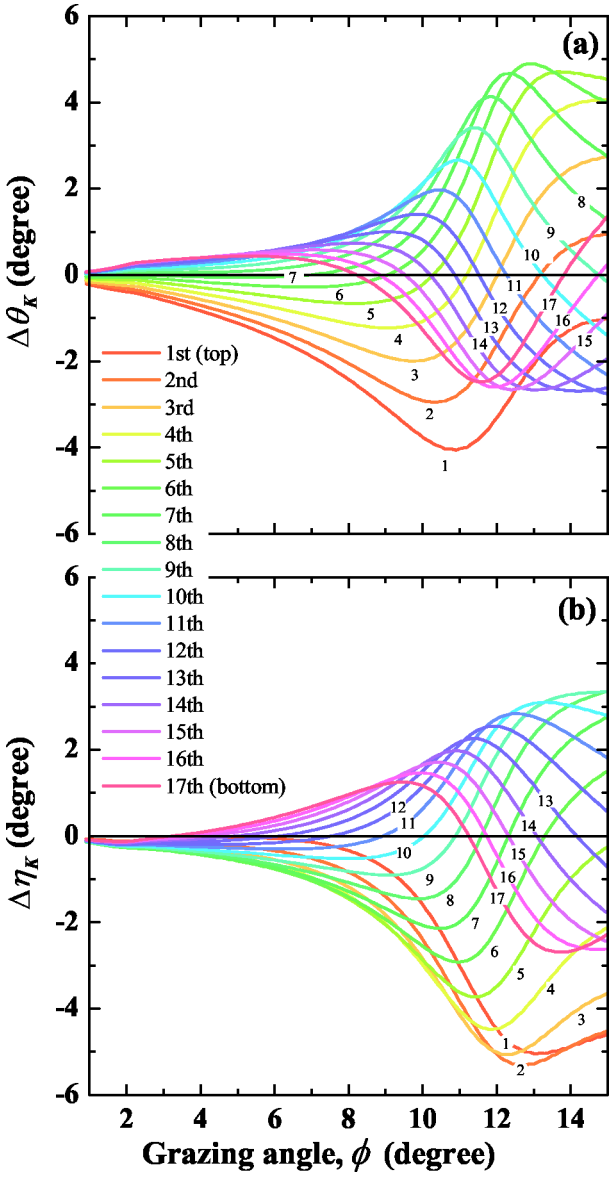

FIG. 7. (Color online) Calculated values of $\Delta\theta_K$ and $\Delta\eta_K$ as a function of ϕ for the individual spin flips of 17-layer-divided regions in a single Co layer from a model structure of Si/SiO_2(1500 Å)/Co(35 Å)/Pd(15 Å). The value of $h\nu$=777.8 eV just below the Co L_3 edge is used.

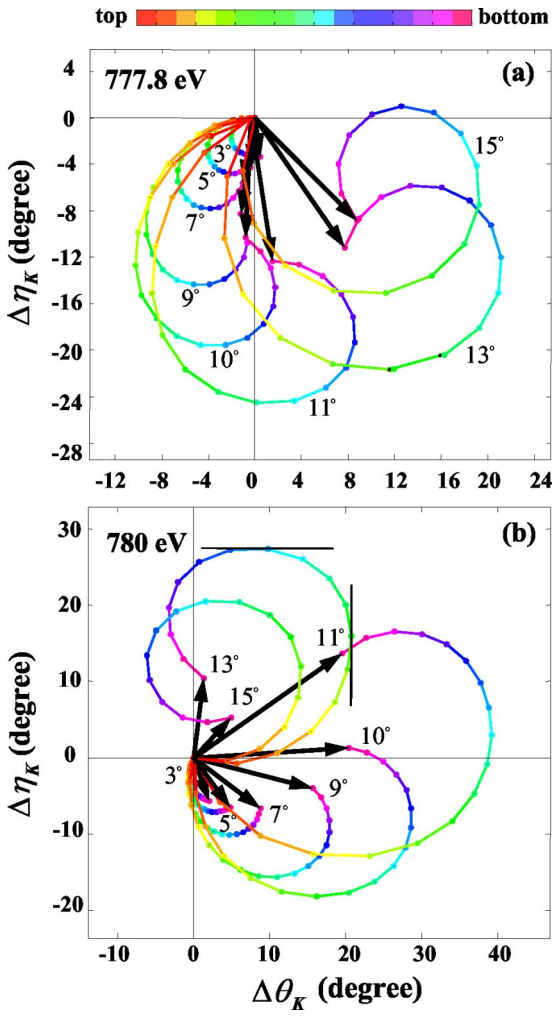

FIG. 8. (Color online) Trace curves of the individual Kerr vectors on the θ_K-η_K plane contributed from each region of the 17 layers being divided in a single Co layer at $h\nu$=777.8 eV in (a) and 780 eV in (b). The first Kerr vector starting from zero point is the Kerr vector contributed from the top region for its spin flip. The sample structure is the same as that used in Fig. 7.

cal representation of the Kerr vector on the θ_K-η_K plane. The overall Kerr vector for a given magnetic layer results from all the MOKE contributions from individual regions being divided in the entire thickness, and hence can be expressed by the sum of complex Kerr vectors contributed from the individual jth regions at the corresponding depths as $\Sigma_j\theta_K^j + i\eta_K^j = \Sigma_j A_j e^{i\Psi_j}$, where A_j is the Kerr amplitude and Ψ_j is the phase.[19] Figure 8 shows the individual Kerr vectors as well as their sums calculated for different ϕ values at $h\nu$=777.8 and 780 eV. The magnitude and orientation of the individual Kerr vectors on the curved lines indicate the weight of individual contributions to the overall Kerr vectors denoted by the large black arrows. For a given jth region within the Co layer, the components of the jth Kerr vector projected on the θ_K and η_K axes represent the degree of the sensitivity of θ_K^j and η_K^j, respectively. The different shapes and sizes of the trace curves for ϕ=3°, 5°, 7°, 9°, 10°, 11°, 13°, and 15° at both $h\nu$=777.8 and 780 eV represent remarkably changing weight of the depth sensitivity depending on ϕ and $h\nu$.

From those trace curves, one can extract valuable information on to what extent each depth contributes to the overall Kerr vector depending on ϕ and $h\nu$. For example, for the trace curve of $h\nu$=780 eV and ϕ=13°, the horizontal line of the 11th region (i.e., $d\Delta\eta_K/d\Delta\theta_K$=0) means $\Delta\eta_K \sim 0$, indicating that any spin flip in this region cannot be detected through η_K signals. Also, in the same condition the vertical line (i.e., $d\Delta\eta_K/d\Delta\theta_K \sim \infty$) shows $\Delta\theta_K \sim 0$ so that any spin flip in that region cannot be detected using θ_K signals. Consequently, tangential lines on the trace curves at given depth regions, which are varying with ϕ and $h\nu$, are very informative to determine which region in a magnetic layer mostly contributes to the overall Kerr effect resulting from the entire thickness. As seen in Fig. 8, the graphical representation of the traces of individual Kerr vectors is very useful for a better understanding of the underlying physics of the depth sensitivity and a guide to choose θ and $h\nu$ suitable for resolving the individual **M** reversals of specific depth regions from the overall **M** reversal.

[This article is copyrighted as indicated in the article. Reuse of AIP content is subject to the terms at: http://scitation.aip.org/termsconditions. Downloaded to] IP: 114.70.7.203 On: Mon, 27 Oct 2014 02:28:35

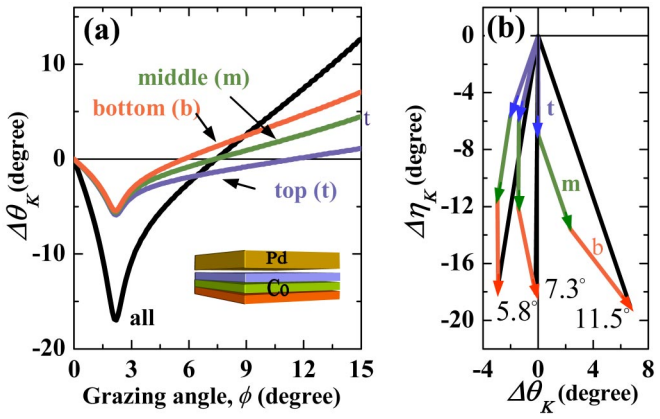

FIG. 9. (Color online) (a) Calculated values of $\Delta\theta_K$ as a function of ϕ for $h\nu$=778.1 eV for the individual spin flips of top, middle, and bottom regions in the 6-Å-thick Co layer of a Si/SiO_2(1500 Å)/Co(6 Å)/Pd(15 Å) structure. (b) Their vector sums of the individual complex Kerr vectors contributed from the three different regions.

E. Atomic-scale depth sensitivity

In order to examine the extent of the depth resolution of the Kerr effect, we also calculate $\Delta\theta_K$ vs ϕ for $h\nu$ =778.1 eV from a simpler layered structure with a thinner magnetic layer, Si/SiO_2(1500 Å)/Co(6 Å)/Pd(15 Å). Figure 9(a) shows the resultant $\Delta\theta_K$ vs ϕ for the individual spin flips of top, middle, and bottom regions with a 2-Å thickness in the 6-Å-thick Co layer. The Co layer is thin enough to examine whether an atomic-scale resolution can be obtained from such a thin layer.

For a spin flip of the bottom region, $\Delta\theta_K$ is almost zero at ϕ=5.8°, while the value of $\Delta\theta_K$ is largest for the top spin flip. This indicates that any spin flip in the bottom region cannot be measured with the given values of ϕ and $h\nu$ via the θ_K signal, but the top spin flip can be resolved because of its largest contribution to the overall $\Delta\theta_K$. In contrast with ϕ=5.8°, the top and bottom spin sensitivities are reversed for ϕ=11.5°. We can thus resolve **M** reversals from a specific depth region of interest even in such a few monolayer thick films by choosing appropriate values of ϕ and $h\nu$ in the θ_K measurements.

In Fig. 9(b), we also display a vectorial representation of the individual Kerr vectors contributed from the three different regions for ϕ=5.8°, 7.3°, and 11.5°. As mentioned earlier, this vector representation allows us to better understand the degree of depth selectivities at different values of ϕ, as well as informs on which values of ϕ and $h\nu$ should be selected to resolve **M** reversals at specific depth regions of interest. For instance, $\Delta\theta_K$ values for bottom, middle, and top spin flips are almost zero at ϕ=5.8°, 7.3°, and 11.5°, respectively. These calculations clearly verify that the resonant Kerr effect is sensitive to depth at the atomic scale even in a few monolayer thick layer.

F. Effect of overlayer thickness on the depth sensitivity of θ_K

As mentioned earlier, the depth sensitivity of the Kerr effect changing with ϕ and $h\nu$ is associated with a rich variety of the interference effect superimposed with the resonant magneto-optical effects that are both varying with ϕ and $h\nu$. Related to this point, to examine the effect of overlayer thickness on the sensitivity as well as to learn how the overlayer effect enhances the depth sensitivity, we calculate $\Delta\theta_K$ for the individual spin flips of top, middle, and bottom regions in a 30-Å-thick Co layer for various thicknesses t of a Pd overlayer, as shown in Fig. 10(a).

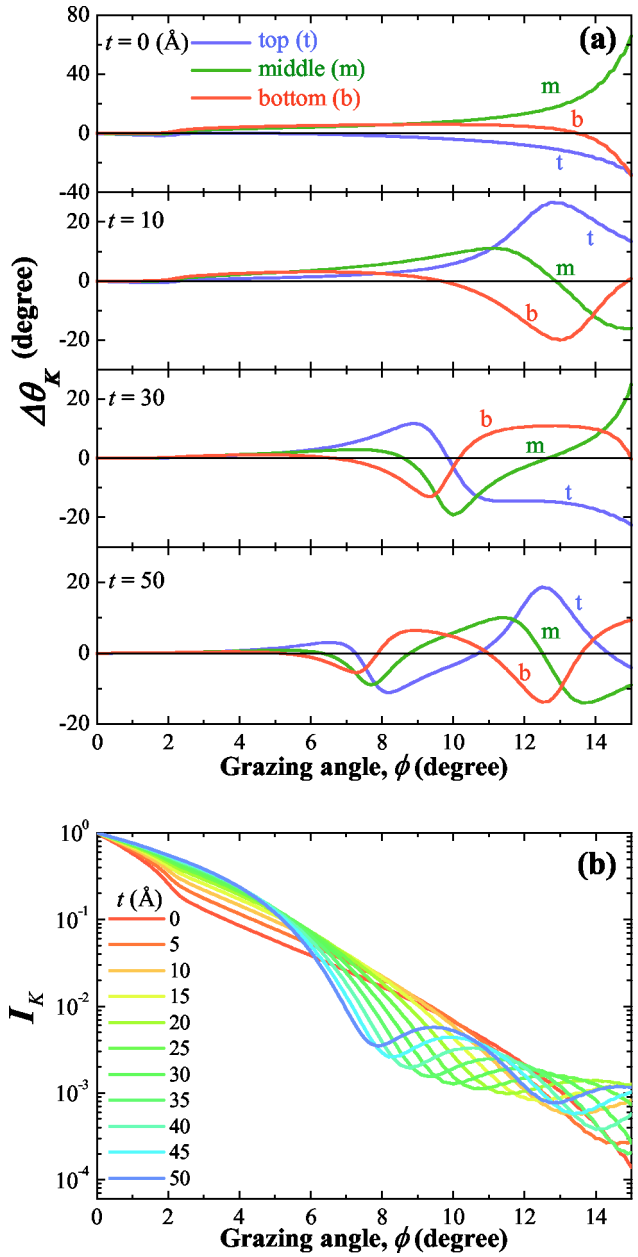

FIG. 10. (Color online) (a) Calculations of the effect of overlayer thickness on $\Delta\theta_K$ sensitivity to three different regions in the ultrathin Co layer of Si/SiO_2(1500 Å)/Co(30 Å)/Pd(t Å), where the Pd thickness varies as t =0, 10, 30, and 50 Å. For the calculations, $h\nu$=781.5 eV is used. (b) Reflected intensities as a function of ϕ from the same structure as that used in (a), but t varies from 0 to 50 Å in a step of 5 Å.

Resultant $\Delta\theta_K$ values are dependent on ϕ and strongly enhanced at certain values of ϕ. For t=0 Å, $\Delta\theta_K$ for all the three different depths increase with ϕ in its magnitude. As t increases, resonant features become stronger, as well as the number of oscillation peaks increases. Such oscillatory behaviors can be characterized roughly by their frequency and

[This article is copyrighted as indicated in the article. Reuse of AIP content is subject to the terms at: http://scitation.aip.org/termsconditions. Downloaded to] IP: 114.70.7.203 On: Mon, 27 Oct 2014 02:28:35

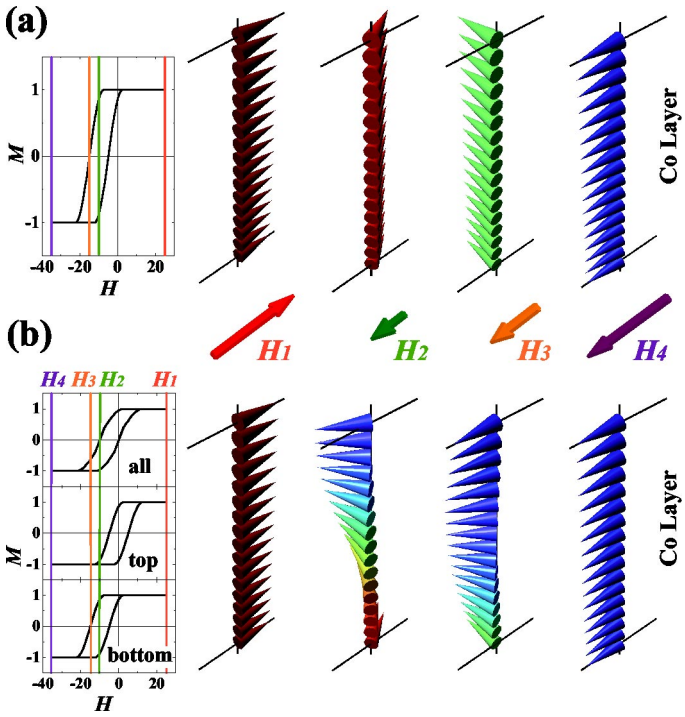

FIG. 11. (Color online) Two models of magnetization reversals in response to applied magnetic fields. (a) Uniform (coherent) and (b) nonuniform (incoherent) reversal in depth in the 35-Å-thick Co layer of a model structure of $Si/SiO_2(1500\ Å)/Ta(50\ Å)/Ni_{81}Fe_{19}(80\ Å)/Fe_{50}Mn_{50}(200\ Å)/Co(35\ Å)/Pd(15\ Å)$. Model hysteresis loops for the individuals are shown in the left-side panels. In (b) the top region traces a symmetric loop while the bottom follows an asymmetric (exchange biased) loop. The color-coded arrows indicate the relative size and the direction of the applied magnetic fields marked by the same color-coded vertical lines shown in the hysteresis loops.

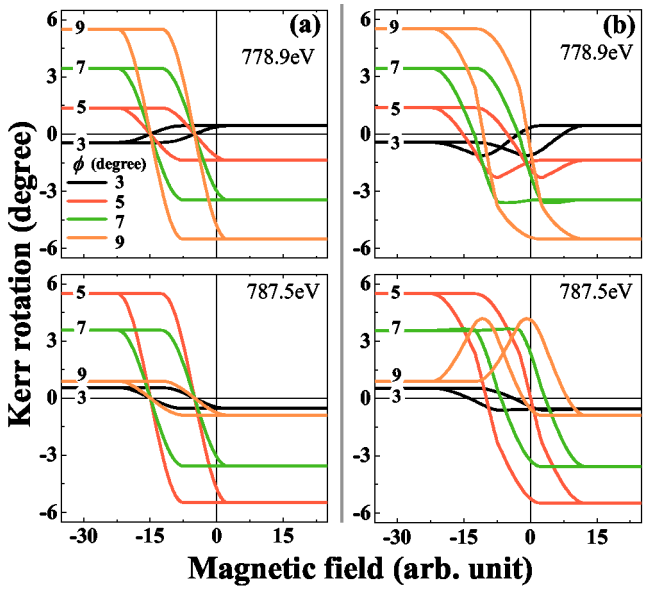

FIG. 12. (Color online) Calculations of θ_K loops based on the two models of (a) coherent and (b) incoherent reversals illustrated in Fig. 11 at various values of ϕ and $h\nu$ as noted.

amplitude. The various frequencies in the oscillations lead to a large difference in $\Delta\theta_K$ between the individual depths, thus enhancing the sensitivity to depth.

The oscillatory features are related to the variation of t, which comes from the variation of the interference effect depending on t. Since the Pd overlayer contributes to the whole interference effect in the entire layered structure, the resonant features in $\Delta\theta_K$ vs ϕ and its dependence on t are ascribed primarily to the interference effect changing with t. Here, we suggest that the overlayer effect offers a much improved depth sensitivity through the overlayer-assisted interference effect.

G. θ_K hysteresis loops calculated from model structures

We can calculate θ_K hysteresis loops from model spin structures. The two distinct models of uniform (coherent) and nonuniform (incoherent) magnetization reversals are illustrated in Fig. 11. The contrasting spin configurations for the two different coherent and incoherent reversals lead to their characteristic hysteresis loops, as illustrated in the left side of Fig. 11. For the coherent rotation, **M** orientations simultaneously rotate through the entire thickness (all spins are equally exchange-biased in the model). For the other incoherent case in Fig. 11(b), we assume that a top spin follows a symmetric (no loop bias) reversal while a bottom spin follows an asymmetric (loop bias) reversal, because the bottom spin is coupled to AF spins. Thus, individual spins present between the top and bottom gradually rotate in the entire thickness due to an exchange coupling between them, as shown in Fig. 11(b). The characteristic overall loop for the incoherent reversal shown in the left side of Fig. 11(b) is exchange biased. In contrast with the spin-flip model mentioned earlier, these two models have the transverse components of **M**, which are changing according to the applied magnetic fields.

Since a remarkable depth sensitivity of θ_K and its dependence on ϕ and $h\nu$, θ_K loops are expected to be field-shifted and those field shifts would be dependent on ϕ and $h\nu$ for the incoherent reversal. In contrast, loops for the coherent case are expectedly placed at the exchange bias field even for different values of ϕ and $h\nu$. Figures 12(a) and 12(b) show the resultant loops for ϕ=3°, 5°, 7°, and 9° with different photon energies $h\nu$=778.9 and 787.5 eV for both models. For the uniform reversal, all the loops show the same field shift, rather resemble its own model loop shown in Fig. 11(a). However, the sign and magnitude of θ_K contrasts can vary with ϕ and $h\nu$. This calculation clearly evidences different loop shifts do not occur if a uniform reversal through the entire thickness is incorporated in real samples. On the other hand, a nonuniform reversal definitely leads to unequal loop shifts according to different values of ϕ and $h\nu$. Owing to the different weights of the depth sensitivity of the Kerr effect depending on ϕ and $h\nu$, the magnitude of the θ_K contrasts from specific depth regions can be enhanced or reduced at a given condition of ϕ and $h\nu$. Consequently, different values of ϕ and $h\nu$ chosen in the measurements can lead to various field shifts. Interestingly, butterflylike but asymmetric loops are also found due to comparable contributions from both top and bottom spins and their opposite sense.

[This article is copyrighted as indicated in the article. Reuse of AIP content is subject to the terms at: http://scitation.aip.org/termsconditions. Downloaded to] IP: 114.70.7.203 On: Mon, 27 Oct 2014 02:28:35

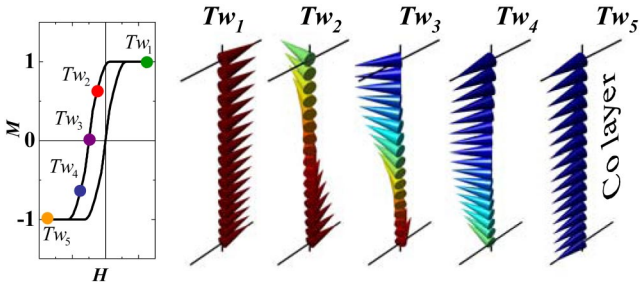

FIG. 13. (Color online) Overall hysteresis loop for an incoherent reversal case. Various spin configurations present during the reversal are illustrated according to the different magnetic fields noted by the color-coded solid circles on the loop.

H. Soft x-ray resonant I_K, θ_K, and η_K spectra versus ϕ as a depth-sensitive probe

In our earlier experiments,[12] we observed various field shifts of hysteresis loops measured through θ_K signals, depending on ϕ and $h\nu$ from a sample with the atomic-scale uniformity of individual constituent layers. It was found that such unusual loop shifts are due to a depth-sensitive property of the Kerr effect combined with depth-varying magnetization reversals present in the sample. Hence, it is interesting how to refine such depth-varying spin configurations during **M** reversals. Here, we suggest that soft x-ray resonant I_K, θ_K, and η_K spectra versus ϕ implicate valuable information on the depth-varying **M** orientations. Keeping it in mind, we calculate I_K, θ_K, and η_K spectra versus ϕ for several different spin configurations using a spin twist model illustrated in Fig. 13. Figure 13 shows a characteristic overall loop for the twist reversal model together with several twist spin configurations at given fields as noted by Tw_1, Tw_2, Tw_3, Tw_4, and Tw_5. Figure 14 shows the resultant I_K, θ_K, and η_K spectra at the Co L_3 and L_2 edges, i.e., $h\nu$=778.1 eV in (a) and 793.3 eV in (b). The I_K spectra for an incident *s*-polarized wave show their negligible difference between individual spin configurations even at the resonance edges. The asymmetry ratio of I_K spectra for Tw_1 and Tw_3 configurations shown in each inset indicates that their structure difference can be discriminated by measured intensities in a range of ϕ=12°~13.5°. This I_K contrast between Tw_1 and Tw_3 is due to the difference in their longitudinal **M** components, not the difference in the transverse **M** components in the light of *s* polarization. Strikingly interesting features are the large variation of θ_K and η_K with varying ϕ and their distinctly different spectra depending on the individual spin configurations. These spectra are also changing remarkably with $h\nu$, as compared between the Co L_3 and L_2 edges. It is very informative that θ_K or η_K spectra versus ϕ remarkably change with details of depth-varying spin structures, thus can be used to make a refinement of those depth-varying structures by fitting experimental spectra to those calculated from various model structures. This technique is very promising as a depth-sensitive probe and becomes a way to refine depth-varying spin structures if such spectra can be readily measured from real samples.

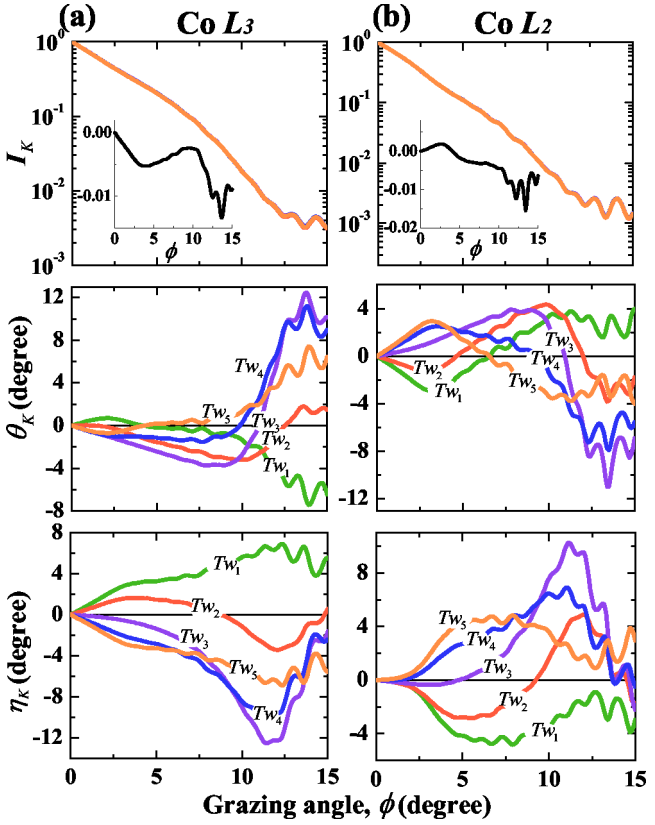

FIG. 14. (Color online) Calculated results of I_K, θ_K, and η_K spectra for $h\nu$ =778.1 (the Co L_3 edge) in (a) and 793.3 eV (the Co L_2 edge) in (b) from each of the different spin configurations illustrated in Fig. 13. The model structure used is the same as Si/SiO_2(1500 Å)/Ta(50 Å)/$Ni_{81}Fe_{19}$(80 Å)/$Fe_{50}Mn_{50}$(200 Å)/Co(35 Å)/Pd(15 Å). The color-coded lines represent those spectra calculated from individual spin configurations noted by Tw_i given at various values of *H* shown in Fig. 13. The I_K spectra are almost the same for the different spin configurations, but asymmetry ratio for the Tw_1 and Tw_3 configurations is as large as ~1.5% around ϕ=12°~13.5°, as shown in each inset.

IV. DEPTH-DEPENDENT SPIN STRUCTURES IN REAL SAMPLES

Magnetic heterostructures have been typically found in various classes of real samples. For example, a nonuniform exchange bias in an ultrathin Co layer of NiFe/FeMn/Co/Pd films was observed by soft x-ray resonant Kerr rotation measurements in our earlier work.[12] We suggested that this nonuniform exchange bias is associated with different strengths of exchange biasing at the FeMn/Co and Co/Pd interfaces. The interfacial Co is strongly exchange biased to the FeMn layer at the FeMn/Co interface but is not (or at least weakly) exchange biased at the Co/Pd interface. This leads to a springlike (twist) spin structure during the reversal. Such a depth-varying spin structure, however, has not been fully determined yet. Those experimental results in our earlier work just indicate the presence of a certain depth-varying structure in the ultrathin Co layer, possibly parts of a springlike spin structure during the reversal. Further study is thus necessary to determine the exact spin structure.

Another springlike spin structures in an AF layer was also suggested in oppositely exchange biased F/AF/F trilayer films of a structure of NiFe(200 Å)/FeMn(t_{AF})/Co(100 Å) with varying t_{AF}.[20] In this work, the existence of a springlike

[This article is copyrighted as indicated in the article. Reuse of AIP content is subject to the terms at: http://scitation.aip.org/termsconditions. Downloaded to] IP: 114.70.7.203 On: Mon, 27 Oct 2014 02:28:35

spin structure within the AF FeMn layer is proposed to explain the oppositely oriented exchange bias between the two F layers with the single AF layer. However, a direct experimental evidence for the springlike spin structure has not been reported yet because of the difficulty in probing depth-resolved *compensated* AF spin structures. Quite recently, twist spin structures involved in AF layers have been confirmed directly by x-ray magnetic linear dichroism spectroscopy.[21] Here, we notice that such springlike structures possibly present in both F and AF layers would cause to reduce exchange bias strengths, according to the model proposed by Mauri *et al.*[22] Such depth-varying spin structures in F or AF layers would be a key to unveil the exchange bias origin.

Also, spring magnet systems consisting of soft and hard magnetic layers exhibit springlike spiral structures in soft magnetic layers.[23] The pinned spins at hard/soft magnet interfaces can cause the springlike configurations during **M** reversals driven by an applied magnetic field. As explained above, many types of depth-varying spin structures have been observed in real samples, so that it is very important to clearly unveil those fine structures in order to correlate them with their overall magnetic properties.

V. SUMMARY

The model simulations in the present work confidently support that the x-ray resonant MOKE is extremely sensitive to depth in an ultrathin magnetic layer and that the depth sensitivity varies remarkably with the grazing angle of incidence and photon energy near the resonance regions. In addition, an atomic-scale depth resolution of the Kerr effect can be obtained in some cases. Such properties of the Kerr effect as a depth-sensitive probe of magnetic heterogeneity are examined through various model simulations including spin-flip reversals and twist spin configurations during **M** reversals. A graphical representation of individual Kerr vectors contributed from each depth region in an ultrathin layer is a very useful way to better understand and clarify the characteristics of the depth sensitivity. These properties of the Kerr effect are associated closely with a rich variety of the wave interference effect superimposed with the resonant optical effect that are both varying significantly with the grazing angle and photon energy of soft x rays near the resonance regions. Here, we used an *s* polarization of incident waves. The other polarization was reported elsewhere.[24]

In conclusion, soft x-ray resonant magneto-optical Kerr effect is promising as a depth-sensitive probe of magnetic heterogeneity in multicomponent multilayer structures with an element specificity and an atomic-scale depth resolution. The Kerr rotation, ellipticity, as well as intensity measurements versus the grazing angle of incidence or photon energy will be a newly emerging powerful way in order to confidently unveil a variety of spin structures varying in depth during **M** reversals in a large variety of magnetic heterostructures currently used in practical spintronic devices.

ACKNOWLEDGMENTS

This work was supported by the Basic Research Program under Grant No. R08-2003-000-10410-0. A few figures in this paper are reproduced from some figures reported in Ref. 12.

[1] J. B. Kortright, D. D. Awschalom, J. Stöhr, S. D. Bader, Y. U. Idzerda, S. S. P. Parkin, I. K. Schuller, and H.-C. Siegmann, J. Magn. Magn. Mater. **207**, 7 (1999).
[2] S. S. P. Parkin *et al.*, J. Appl. Phys. **85**, 5828 (1999).
[3] S. A. Wolf, D. D. Awschalom, R. A. Buhrman, J. M. Daughton, S. von Molnár, M. L. Roukes, A. Y. Chtchelkanova, and D. M. Treger, Science **294**, 1488 (2001).
[4] S.-K. Kim and J. B. Kortright, Phys. Rev. Lett. **86**, 1347 (2001).
[5] S. H. Yang *et al.*, J. Phys.: Condens. Matter **14**, L407 (2002).
[6] J. Nogues and I. K. Schuller, J. Magn. Magn. Mater. **192**, 203 (1999).
[7] J. B. Kortright and S.-K. Kim, Phys. Rev. B **62**, 12216 (2000).
[8] J. B. Kortright, S.-K. Kim, E. E. Fullerton, J. S. Jiang, and S. D. Bader, Nucl. Instrum. Methods Phys. Res. A **467–468**, 1396 (2001).
[9] O. Hellwig, J. B. Kortright, K. Takano, and E. E. Fullerton, Phys. Rev. B **62**, 11694 (2000).
[10] H.-Ch. Mertins, S. Valencia, D. Abramsohn, A. Gaupp, W. Gudat, and P. M. Oppeneer, Phys. Rev. B **69**, 064407 (2004); H.-Ch. Mertins, D. Abramsohn, A. Gaupp, F. Schäfers, W. Gudat, O. Zaharko, H. Grimmer, and P. M. Oppeneer, Phys. Rev. B **66**, 184404 (2002); H.-Ch. Mertins, P. M. Oppeneer, J. Kuneš, A. Gaupp, D. Abramsohn, and F. Schäfers, Phys. Rev. Lett. **87**, 047401 (2001).
[11] J. L. Erskine and E. A. Stern, Phys. Rev. B **12**, 5016 (1975).
[12] K.-S. Lee, S.-K. Kim, and J. B. Kortright, Appl. Phys. Lett. **83**, 3764 (2003); Some results of calculations reported in the above paper have an error of the sign convension in θ_K and η_K in computer coding, but the error has been corrected in the present paper.
[13] R. Nakajima, J. Stöhr, and Y. U. Idzerda, Phys. Rev. B **59**, 6421 (1999).
[14] Z. J. Yang and M. R. Scheinfein, J. Appl. Phys. **74**, 6810 (1993).
[15] J. Zak, E. R. Moog, C. Liu, and S. D. Bader, J. Magn. Magn. Mater. **89**, 107 (1990).
[16] Z. Q. Qiu and S. D. Bader, J. Magn. Magn. Mater. **200**, 664 (1999).
[17] The absorptive (β) and refractive (δ) parts of n are corelated through the KKT. The used values of the refractive indices were measured from thin films of magnetic elements. For details, see Ref. 7. For a few monolayer thick films, of course, these refractive indices can be altered in their values due to modified electronic structures at buried interfaces.
[18] B. L. Henke, E. M. Gullikson, and J. C. Davis, At. Data Nucl. Data Tables **54**, 181 (1993); Numerical data can be found at http://www-cxro.lbl.gov
[19] J. Hamrle, J. Ferré, M. Nývlt, and Š. Višňovský, Phys. Rev. B **66**, 224423 (2002).
[20] F. Y. Yang and C. L. Chien, Phys. Rev. Lett. **85**, 2597 (2000).
[21] A. Scholl, M. Liberati, E. Arenholz, H. Ohldag, and J. Stöhr, Phys. Rev. Lett. **92**, 247201 (2004).
[22] D. Mauri, H. C. Siegmann, P. S. Bagus, and E. Kay, J. Appl. Phys. **62**, 3047 (1987).
[23] E. E. Fullerton, J. S. Jiang, M. Grimsditch, C. H. Sowers, and S. D. Bader, Phys. Rev. B **58**, 12193 (1998).
[24] K.-S. Lee, S.-K. Kim, and J. B. Kortright, J. Appl. Phys. **96**, 7414 (2004).

[This article is copyrighted as indicated in the article. Reuse of AIP content is subject to the terms at: http://scitation.aip.org/termsconditions. Downloaded to] IP: 114.70.7.203 On: Mon, 27 Oct 2014 02:28:35